2021 43rd Annual International Conference of the
IEEE Engineering in Medicine & Biology Society (EMBC)
Oct 31 - Nov 4, 2021. Virtual Conference

Computational Fluid Dynamics (CFD) Analysis of Subject-specific Bronchial Tree Models in Lung Cancer Patients

L. Aliboni, F. Pennati, M. Sarti, V. Iorio, R. Carrinola, A. Palleschi, and A. Aliverti

Abstract— **Lung resection is the only potentially curative treatment for lung cancer. The inevitable partial removal of functional lung tissue along with the tumoral mass requires a careful and structured pre-operative condition of patients. In particular, the postoperative residual functionality of the lung needs to be predicted. Clinically, this is assessed through algorithms based on pulmonary function tests (PFTs). However, these approaches neglect the local airway segment's functionality and provide a globally averaged evaluation. CFD was demonstrated to provide patient-specific, quantitative, and local information on flow dynamics and regional ventilation in the bronchial tree. This study aims to apply CFD to characterize the flow dynamics in 12 patients affected by lung cancer and evaluate the effects of the tumoral masses on flow parameters and lobar flow distribution. Patient-specific airway models were reconstructed from CT images, and the tumoral masses were manually segmented. Measurements of lungs and tumor volumes were collected. A peripherality index was defined to describe tumor distance from the parenchyma. CFD simulations were performed in Fluent®, and the results were analyzed in terms of flow parameters and lobar volume flow rate (VFR). The predicted postoperative forced expiratory volume in 1s (ppoFEV1) was estimated and compared to the current clinical algorithm. The patients under analysis showed relatively small tumoral masses located close to the lung parenchyma. CFD results did not highlight lobar alterations of flow parameters, whereas the flow to the lung affected by the tumor was found to be significantly lower ($p=0.026$) than the contralateral lung. The estimation ppoFEV1 obtained through the results of the simulations showed a high correlation ($\rho=0.993$, $p<0.001$) with the clinical formula.**

Clinical Relevance— **The proposed study establishes the efficacy and applicability of CFD for the pre-operative characterization of patients undergoing lobectomy surgery. This technique can provide additional information on local functionality and flow dynamics to support patients' operability.**

I. Introduction

Pulmonary lobectomy is the gold standard curative approach to localized lung cancer, consisting of the resection of a pulmonary lobe [1]. Extensive resection of functional tissue causes a permanent loss of pulmonary function, worsening the condition of candidates that generally have already concomitant pathologies [2]. The prediction of postoperative pulmonary function is crucial for establishing surgical risk and operability of the patient. The current clinical practice relies on PFTs, i.e., spirometry and cardiopulmonary exercise tests [1]. However, none of these methods accounts for volume differences among pulmonary segments and lobes, tissue heterogeneity, and postoperative alterations of lung and airways anatomy [2], [3]. Besides, PFTs provide only global, at-mouth averaged measurements of lung volumes and require patients' collaboration. CFD represents an attractive tool to address some of the limitations of current clinical approaches by providing quantitative information on regional ventilation, lobar flow rate, and local properties at every location in the airways [4]–[6]. The fluid dynamics effects of pulmonary lobectomy were recently studied for the left upper lobectomy case [7], [8], focusing on comparing the pre and postoperative conditions. The study aims to investigate flow characteristics in subjects prior to lobectomy surgery to identify possible flow alterations induced by the tumoral mass. Also, the lobar flow rate obtained through CFD was adopted to calculate ppoFEV1 and compared it to the current clinical algorithm.

II. Materials and Methods

A. Study population

12 Patients (age=74±4, FEV1p=101±18, FVCp= 108±19) affected by carcinoma and adenocarcinoma lung cancer were retrospectively collected. The set of subjects was composed of 7 males and 5 females. 3 patients had the tumoral mass located in the right upper lobe (RUL), 3 in the right lower lobe (RLL), 3 in the left upper lobe (LUL), and 3 in the left lower lobe (LLL). All the patients were positively evaluated for operability and underwent pulmonary lobectomy surgery. Anonymized chest high-resolution CT, acquired in breath-hold at full-inspiration within 3 months before the surgery, were analyzed. Informed consent was obtained from all the patients. Scanner settings: tube voltage=100-120 kV; tube current=79–266 mA according to body mass index; matrix=512x512; slice thickness=0.62–1 mm; in-plane resolution=0.62–0.90 mm; axial resolution=0.6-1.0 mm; reconstruction kernel=B30f.

B. Airways, tumor, and lung segmentation

Airways and lung geometries were automatically reconstructed in Mimics (Materialise NV, BE) up to the 5th generation and successively post-processed in using 3-Matic (Materialise NV, BE) and Ansys SpaceClaim (Ansys Inc., USA). Tumoral mass was manually segmented on each patient.

C. Tumor geometrical characterization

A local peripherality index related to the distance of the tumor from the lung parenchyma was computed as:

$$P = d1 / (d1+d2). \quad (1)$$

L. A., F. P., M. S., V. I., and A. A. are with the Department of Information, Electronics and Bioengineering, Politecnico di Milano, Milan, 20133, IT (corresponding author – L. A. phone: 0039-02-2399-9026; e-mail: lorenzo.aliboni@ polimi.it).

R.C. and A. P. are with the University of Milan, Department of Pathophysiology and Transplantation, Milan, 20100, IT and with the Thoracic Surgery and Lung Transplantation Unit, Fondazione IRCCS Ca' Granda Ospedale Maggiore Policlinico of Milan, Milan, 20100, IT

978-1-7281-1178-0/21/$31.00 ©2021 IEEE

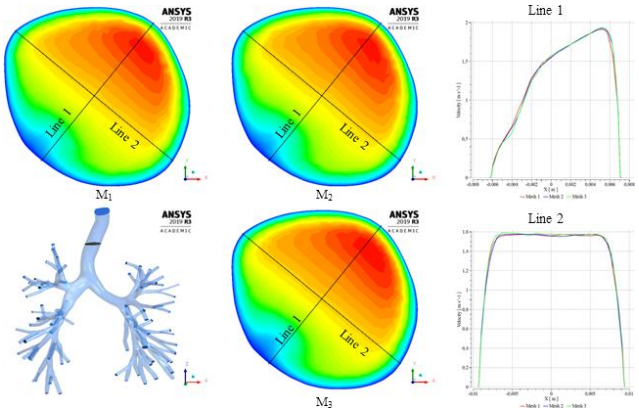

Figure 1. Mesh converge analysis for a representative subject. The location of the plate and its velocity contours (left) and the velocity profile plot along lines 1 and 2 (right) are reported for M1, M2, M3

Where d1 is the distance of the center of gravity (CoG) of the tumoral mass to the main lobe bifurcation of the lobe in which the tumor is located; d2 is the projection on the pleura of CoG in the direction of d1. The percentual volume ratios (R_1, R_2) between the dimensions of the tumor (Vtumor) and the affected lobe (Vlobe) and lung (Vlung) were computed as follows:

$$R_1 = (Vtumor / Vlobe) \times 100 \quad (2)$$

$$R_2 = (Vtumor / Vlung) \times 100. \quad (3)$$

D. Mesh Generation

Tetrahedral unstructured grid meshes were automatically generated for each geometry in Fluent®.15 inflation layers were created to resolve fluid flow properties in the sub-viscous layer proximal to the wall. The first layer thickness was set equal to 0.01 mm, which corresponded to an estimated y+ < 1. Mesh quality was evaluated through the maximum skewness criterion (equilateral volume skewness < 0.90).

Convergence analysis was performed on three meshes (M1, M2, M3) with an increasing number of elements. The average (± SD) number of elements was equal to 3.1×10^6 (± 0.6×10^6), 5.2×10^6 (± 1.2×10^6), 9.8×10^6 (± 2.5×10^6) for M1, M2, M3, respectively. The convergence analysis was conducted considering the relative variations between the meshes in terms of VFR at the outlets, with a tolerance inferior to 0.5%. The local velocity profile was also evaluated for the three meshes at a cross-sectional plane located halfway in the trachea. Two axes, mutually rotated at 90° from each other, were chosen to plot the profiles (Fig. 2). Results were proved to be mesh-independent for all subjects.

E. CFD simulations

Numerical simulations were performed using the finite volumes method for solving the mass conservation and the Navier-Stokes equations in the 3D domain. The effects of turbulence were modeled using the Shear Stress Transport (SST) k-ω model with Low Reynolds Number correction. The model is considered the most suitable model for predicting low turbulence flow in the respiratory system, with limited computational resources [6], [9]. The influence of oscillatory behavior on the flow was preliminarily investigated. The effects of unsteadiness on the average flow characteristics, computed through a steady solution, are modest if the Womersley number (Wo) and the Strouhal number (S) are lower than 10 and 1, respectively [10]. The Wo number, i.e., the ratio of unsteady forces to viscous forces, was calculated as:

$$Wo = D_{ht} / 2 \times (2\pi f/\upsilon)^{0.5} \quad (4)$$

The S number, i.e., the ratio of unsteady forces to inertial forces, was calculated as:

$$S = (2\pi f D_{ht}) / \bar{u} \quad (5)$$

Where f was the breathing frequency, υ is the air kinematic viscosity, Dht was the hydraulic diameter of the trachea, and ū was the average velocity at the corresponding diameter.
f=15 breaths per minute and $\upsilon=1.79\times10$-5 kg/ms were assumed. Dht was measured at the inlet cross-section for all the models, while the velocity at the trachea was obtained by dividing the inlet flow rate by the inlet cross-section. The inspiratory flow was assumed to equal 0.5 L/s, simulating the peak inspiratory flow during quiet breathing. The average Womersley and Strouhal numbers were equal to 2.25 (± 0.25) and 0.010 (± 0.005), respectively. Consequently, a steady inspiratory flow (0.5 L/s) was set as a boundary condition at the trachea inlet. A turbulent intensity of 5% and a viscosity ratio of 10 were applied. Uniform reference pressure was set at each outlet boundary, corresponding to the cross-sectional surface at the terminal end of each bronchus. A no-slip condition was imposed at the walls, considered rigid, stationary, and smooth. The air was assumed to be an incompressible Newtonian fluid, with density and dynamic viscosity equal to 1.225 kg/m3 and $1.79 \times 10{-}5$ kg/ms. This assumption is acceptable for the airflow in the human airways, where the Mac number is close to 0.3, and the effects of temperature and humidity cause negligible variations on the air properties with respect to environmental conditions [10], [11]. The following numerical methods were adopted: pressure-based solver; second-order upwind scheme for the momentum equations; Green-Gauss cell-based method for gradients evaluation; and semi-implicit method for pressure linked equations algorithm for pressure-velocity coupling. Convergence was set as residuals less than 10^{-6}. Calculations stopped when the residuals converged, and the solution was stable. The results were reported in terms of velocity magnitude, wall pressure, and wall shear stress, in the entire tree. The pressure drop between the inlet and the outlets was also computed.

F. Estimation of postoperative lung function

The estimation of the postoperative function (ppoFEV1) has been performed in accordance with the current clinical guidelines [1], using the anatomical method [12]:

$$ppoFEV1 = pre\text{-}opFEV1 \times (1 - y / z) \quad (6)$$

Where y is the number of functional or unobstructed lung segments to be removed, and z is the total number of

functional segments. The total number of segments is assumed to equal 10 for the right lung (3 RUL, 3 in the right middle lobe (RML) and in the RLL), and 9 for the left lung (5 in the LUL, 4 in the LLL) [12]. The ppoFEV1 was computed using the VFR to the healthy lobes (VFR_H) obtained through the numerical solution (7):

$$ppoFEV1_{CFD} = \text{pre-opFEV1} \times (VFR_H) \quad (7)$$

G. Statistical Analysis

Results are reported as median (25^{th}–75^{th} percentile) unless otherwise stated. Correlations were evaluated through Spearman Correlation. Comparisons of parameters between lungs (right/left) and position of the tumor in the upper/lower lobes were analyzed through the Mann-Whitney test. Statistical analysis was performed in IBM SPSS® Statistics 25.0. PFT values were expressed as a percentage of predicted.

III. Results

Results relative to the tumoral mass characterization and the fluid dynamics parameters for each subject were reported in Table 1. Tumoral masses were peripherical, P = 0.85 (0.79-0.89) and small, R1 = 0.4 (0.07 – 0.92) %, R2 = 0.18 (0.03-0.42) %. The VFRs to each lobe were reported in Fig. 2, colored by the site of resection. In general, lower lobes received more flow compared to upper ones, and the right lung (RL) showed higher flow with respect to the left lung (LL). Despite the variability, it can be observed that for a given subset of subjects with a tumor in a specified lobe, the corresponding pathological lobe showed a mild reduction of flow intake than the corresponding healthy lobes of the remaining subjects. This difference was tested to be significant at the level of the full lungs. In the lung characterized by the presence of the tumoral mass, a significant reduction of flow (p= 0.026) compared to the contralateral was observed. The results of the calculation of the ppoFEV1 with the clinically established (6) and with the proposed approach (7) were also reported in Table 1. The

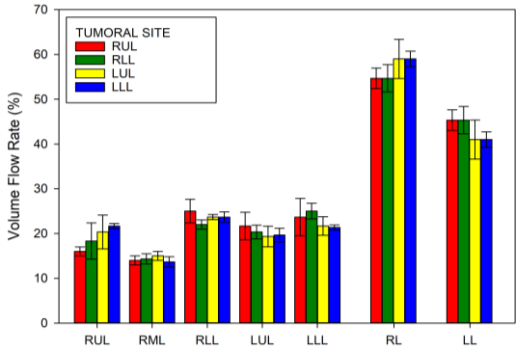

Figure 2. Lobar and lung VFR colored according to the lobe affected by the tumor. RL=right lung, LL= left lung

results obtained with the simulations show a high correlation (0.993, ρ=<0.001) with the anatomical method calculations. No lung or lobe-related differences were identified. The variation of fluid dynamics parameters (Fig. 3) reflected the inter-subject variability in airways geometry. Fluid dynamics did not show specific alterations in the pathological lobe/lung, neither globally nor locally. Velocity streamlines appear relatively smooth, with no large vortex in all models. Indeed, for the patients under analysis, no statistically significant differences in terms of percentual variation of pressure, velocity, wall shear, or pressure drop were observed if grouped for the affected lung or the position of the pathological lobe (upper/lower).

IV. Discussion

The values of fluid dynamics parameters suggest that, overall, the flow distribution does not show significant alterations related to the presence of the tumoral mass. Indeed, not significant global or local differences are observed in the distribution of velocity, pressure, and wall shear stress. This can be possibly related to the relatively small size and the peripherality of the tumoral masses in the patients under analysis. VFR distribution was higher in the lower lobes and the right lung as expected due to their larger dimensions [10]

TABLE I. Results of Tumoral Mass Characterization, CFD Parameters, and Functional Evaluation

ID	Anatomical Characterization				CFD parameter				Functional Evaluation		
	Lobe	*P*	*R1*	*R2*	*Velocity (m/s)*	*Wall Pressure (Pa)*	*Wall Shear Stress (Pa)*	*Pressure Drop (Pa)*	*FEV1 (%)*	*ppoFEV1 (%)*	*ppoFEV1$_{CFD}$ (%)*
1	RUL	0.87	0.11	0.04	2.81	5.29	0.89	3.81	111	93	93
2	RUL	0.89	0.77	0.32	2.08	3.55	0.58	1.67	131	110	111
3	RUL	0.90	0.05	0.02	5.01	19.22	1.64	15.13	71	60	59
4	RLL	0.80	0.31	0.15	3.47	11.86	1.29	4.87	84	62	66
5	RLL	0.86	0.97	0.45	3.73	12.45	0.87	9.14	108	80	83
6	RLL	0.87	0.06	0.02	2.03	5.89	0.54	3.47	102	75	80
7	LUL	0.78	0.32	0.18	4.86	19.19	1.28	13.88	100	74	78
8	LUL	0.84	1.48	0.62	2.67	6.65	0.70	5.38	97	71	80
9	LUL	0.94	0.05	0.03	3.66	9.18	0.83	7.57	86	63	71
10	LLL	0.48	0.49	0.21	4.16	15.56	1.22	12.00	74	58	58
11	LLL	0.69	1.44	0.64	2.52	7.81	0.51	4.86	118	93	93
12	LLL	0.84	0.47	0.17	5.51	16.79	1.84	12.55	125	99	98

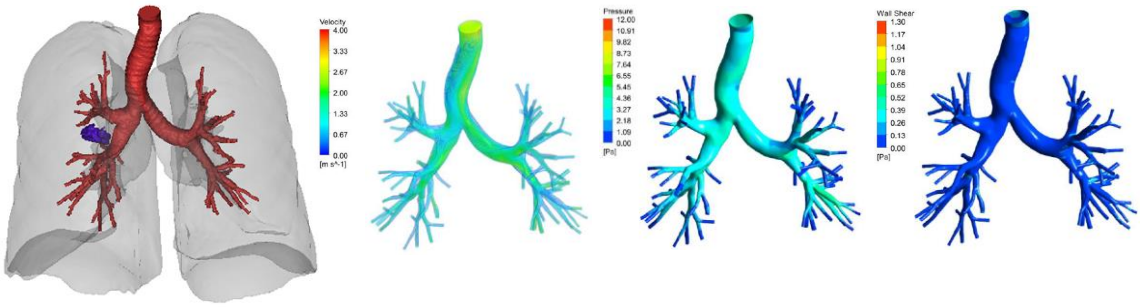

Figure 3. Results of CFD simulation for a representative subject (ID 5). From left to right the reconstruction of the respiratory structures and tumoral mass, the stream lines of velocity, wall pressure and wall shear stress are reported

compared to the upper lobes and the left lung. The RML, being the smaller lobe, received less flow. These considerations are in line with previous computational studies [6], [13], [14]. A significant difference between the lung in which the tumoral mass is located and the contralateral lung is observed in VFR distribution, with the former showing a lower flow intake. The identification of airflow reduction as an independent risk factor for lung cancer has been suggested [16], and our results support this evidence. Also, it has been demonstrated that patients with coexisting moderate-to-severe airflow limitation and emphysema had significantly poorer overall survival after lung resection [15]. The capability to quantify (at a lobar or lung level) the severity of airflow reduction can consequently constitute a helpful insight from a clinical perspective. Also, the calculation of the ppoFEV1 through CFD-estimated VFR showed excellent agreement with the current anatomical formula used in clinical practice. Compared to this latter global formula, however, CFD analysis can provide pre-operative information on the actual functionality of each segment. This information can be of extreme value, especially in evaluating cases in which the current clinical algorithms result in a borderline estimation of patients' operability. This study has some limitations. Expiratory scans were not present as they were not included in the clinical protocol for these patients. They could have provided additional information in applying patient-specific boundary conditions and allowed the simulation of the expiratory condition. Dynamic simulations will have to be introduced, and the dataset, although quite numerous for a computational approach, will need to be extended to confirm possible clinical implications further.

V. Conclusion

This study constitutes the first insight into the application of CFD to investigate pre-operative conditions in lung cancer patients to the best of our knowledge. Future directions of development will address the need for a larger cohort of subjects, the introduction of more patient-specific boundary conditions, and the longitudinal evaluation of patients' postoperative progress in relation to the presented pre-operative information.

Acknowledgment

We thank PARAMETRIC DESIGN SRL for the computational resources.

References

[1] A. Brunelli *et al.*, "ERS/ESTS clinical guidelines on fitness for radical therapy in lung cancer patients (surgery and chemo-radiotherapy)," *Eur. Respir. J.*, vol. 34, no. 1, pp. 17–41, 2009, doi: 10.1183/09031936.00184308.

[2] G. Miserocchi, E. Beretta, and I. Rivolta, "Respiratory Mechanics and Fluid Dynamics After Lung Resection Surgery," *Thorac. Surg. Clin.*, vol. 20, no. 3, pp. 345–357, 2010, doi: 10.1016/j.thorsurg.2010.03.001.

[3] M. J. Licker *et al.*, "Operative Mortality and Respiratory Complications After Lung Resection for Cancer: Impact of Chronic Obstructive Pulmonary Disease and Time Trends," *Ann. Thorac. Surg.*, vol. 81, no. 5, pp. 1830–1837, 2006, doi: 10.1016/j.athoracsur.2005.11.048.

[4] K. S. Burrowes, J. De Backer, and H. Kumar, "Image-based computational fluid dynamics in the lung: virtual reality or new clinical practice?," *Wiley Interdiscip. Rev. Syst. Biol. Med.*, vol. 9, no. 6, pp. 1–16, 2017, doi: 10.1002/wsbm.1392.

[5] J. W. De Backer *et al.*, "Flow analyses in the lower airways: Patient-specific model and boundary conditions," *Med. Eng. Phys.*, vol. 30, no. 7, pp. 872–879, 2008, doi: 10.1016/j.medengphy.2007.11.002.

[6] H. Y. Luo and Y. Liu, "Modeling the bifurcating flow in a CT-scanned human lung airway," *J. Biomech.*, vol. 41, no. 12, pp. 2681–2688, 2008, doi: 10.1016/j.jbiomech.2008.06.018.

[7] M. Tullio, L. Aliboni, F. Pennati, R. Carrinola, A. Palleschi, and A. Aliverti, "Computational fluid dynamics of the airways after left-upper pulmonary lobectomy: a case study," *Int. j. numer. method. biomed. eng.*, vol. n/a, no. n/a, p. e3462, doi: https://doi.org/10.1002/cnm.3462.

[8] Q. Gu *et al.*, "Structural and functional alterations of the tracheobronchial tree after left upper pulmonary lobectomy for lung cancer," *Biomed. Eng. Online*, vol. 18, no. 1, pp. 1–18, 2019, doi: 10.1186/s12938-019-0722-6.

[9] F. Krause, A. Wenk, C. Lacor, W. G. Kreyling, W. Möller, and S. Verbanck, "Numerical and experimental study on the deposition of nanoparticles in an extrathoracic oral airway model," *J. Aerosol Sci.*, vol. 57, pp. 131–143, 2013, doi: 10.1016/j.jaerosci.2012.11.004.

[10] J. Tu, K. Inthavong, and G. Ahmadi., *Computational fluid and particle dynamics in the human respiratory system*. Springer Science & Business Media, 2012.

[11] M. A. Atherton, M. W. Collins, and M. J. Dayer, *Repair and Redesign of Physiological Systems*. WIT Press, 2008.

[12] A. Brunelli, A. W. Kim, K. I. Berger, and D. J. Addrizzo-Harris, "Physiologic evaluation of the patient with lung cancer being considered for resectional surgery: Diagnosis and management of lung cancer, 3rd ed: American college of chest physicians evidence-based clinical practice guidelines," *Chest*, vol. 143, no. 5 SUPPL, pp. e166S-e190S, 2013, doi: 10.1378/chest.12-2395.

[13] S. Miyawaki *et al.*, "A 4DCT imaging-based breathing lung model with relative hysteresis," *J. Comput. Phys.*, vol. 326, pp. 76–90, 2016, doi: 10.1016/j.jcp.2016.08.039.A.

[14] S. Verbanck *et al.*, "Inhaled aerosol distribution in human airways: A scintigraphy-guided study in a 3D printed model," *J. Aerosol Med. Pulm. Drug Deliv.*, vol. 29, no. 6, pp. 525–533, 2016, doi: 10.1089/jamp.2016.1291.

[15] S. Shin *et al.*, "Joint effect of airflow limitation and emphysema on postoperative outcomes in early-stage nonsmall cell lung cancer," *Eur. Respir. J.*, vol. 48, no. 6, pp. 1743–1750, 2016, doi: 10.1183/13993003.01148-2016.

[16] F. Maldonado, B. J. Bartholmai, S. J. Swensen, D. E. Midthun, P. A. Decker, and J. R. Jett, "Are airflow obstruction and radiographic evidence of emphysema risk factors for lung cancer? A nested case-control study using quantitative emphysema analysis," *Chest*, vol. 138, no. 6, pp. 1295–1302, 2010, doi: 10.1378/chest.09-2567.